Structure and Formation of Noninteger and Integer Folded-Chain Crystals of Linear and Branched Monodisperse Ethylene Oligomers

Goran Ungar* and Xiangbing Zeng

Department of Engineering Materials, University of Sheffield, Sheffield S1 3JD, U.K.

Gerald M. Brooke and Shahid Mohammed

Chemistry Department, Science Laboratories, University of Durham, South Road, Durham DH1 3LE, U.K.

Received October 21, 1997; Revised Manuscript Received January 20, 1998

ABSTRACT: The formation of primary crystals and their subsequent structural rearrangements are studied by real-time simultaneous small- and wide-angle X-ray diffraction using linear long-chain alkane $C_{246}H_{494}$ and a long alkane with a methyl branch in the center of the chain $C_{96}H_{193}CH(CH_3)C_{94}H_{189}$. The initial crystals formed below the melting point of the folded chains are noninteger folded (NIF); this means that the layer period in the chain direction is l/p, where l is the extended-chain length and p is a noninteger (presently $1 < p < 2$). Following their formation, the NIF crystals transform to the F2 "integer" form with all chains folded in two in the middle ($p = 2$). While this transformation is very rapid in the branched alkane, it is considerably slower in the linear alkane. From the electron density profiles across the lamellar stacks, it is calculated that the NIF form consists of a crystalline core of the same thickness as that in the once-folded F2 lamellae, but with an additional thick interlamellar amorphous layer containing long uncrystallized chain ends (cilia). In the initial NIF form, half the molecules are folded and fully crystallized. The others traverse the crystal layer only once and are only half-crystallized. It is suggested that the uncrystallized ends (cilia) of these latter molecules are generally too short to be incorported in the crystal and are uneven in length due to the longitudinally random chain attachment during crystal growth. The NIF → F2 transformation involves postcrystallization of the cilia as they reach a length of $l/2$ through chain translation. The rapid transformation in $C_{96}H_{193}CH(CH_3)C_{94}H_{189}$ is believed to be due to the initial preference for "correct" chain attachment, with the branch at the lamellar surface, thus leaving the cilia of length $l/2$ suitable for incorporation into the F2 crystals.

Since the pioneering work on low-molecular fractions of poly(ethylene oxide)[1] and the first synthesis of monodisperse long *n*-alkanes,[2,3] the physical behavior of these model polymers has been studied extensively. Folded- and extended-chain lamellar crystals were obtained. Small-angle X-ray scattering (SAXS) and Raman LAM spectroscopy on solution- and melt-crystallized alkanes have shown that mature crystals have fold lengths equal or very close to integer fractions (IF) of the extended chain length.[4,5] In contrast, real-time SAXS experiments of in-situ melt crystallization revealed that the as-formed crystals, when grown below the folded-chain melting temperature, have a layer period L which is a noninteger fraction (NIF) of the period of extended-chain crystals L_0.[6] Primary NIF crystals with an L-value between L_0 and $L_0/2$ were found to transform subsequently to IF forms via either thickening (to the extended form) or thinning (to the once-folded form with $L = L_0/2$). More recent work on poly(ethylene oxide) (PEO) fractions[7] also showed the presence of NIF as the primary form.

In the present study, we measure the intensity distribution among the different diffraction orders and reconstruct the one-dimensional density profile across the layer stacks of NIF and IF phases. Such profiles contain information on the internal lamellar structure. We are particularly interested in the NIF form since this is poorly understood and since it is believed to represent a model for primary bulk crystallization of polymers.

The experiments described here were performed using normal alkane $C_{246}H_{494}$ and, for the first time, a branched long alkane $C_{96}H_{193}CH(CH_3)C_{94}H_{189}$. For details of the synthesis see ref 8. The in situ SAXS experiments were carried out on Station 8.2 of the Daresbury Synchrotron Radiation Source. A Daresbury quadrant multiwire detector was used for the small-angle range while wide-angle diffraction was recorded simultaneously with a curved linear position-sensitive detector (Inel). The capillary with the sample was held in a modified Linkam hot stage equipped with a cooling unit. Coolant gas flow was balanced against the heater, enabling a cooling rate of ca. 1 °C/s. Isothermal temperature was kept within 0.1 °C. The correction for positional nonlinearity of the quadrant detector was done using the first 22 orders of diffraction from wet rat tail collagen. Two matched third-order polynomials were fitted to the inverse collagen spacings for the two halves of the detector range. The sample-to-detector distance was calibrated using polycrystalline samples of a series of shorter orthorhombic *n*-alkanes with precisely known unit cell lengths. Film recordings were taken to ascertain the lack of preferred orientation. All diffraction intensities were normalized by the beam flux which was monitored by an ionization chamber located behind the specimen. In the case of partially overlapping diffractions, peak positions and areas were determined by numerical curve resolution using mixed Gaussian−Lorentzian profiles. Curve fitting was also used for background subtraction in the range of lowest angles. Other experimental details are described elsewhere.[9]

When cooled to a temperature between the extended-chain and folded-chain melting points (128.6 and about

S0024-9297(97)01539-8 CCC: $15.00
Published on Web 02/26/1998

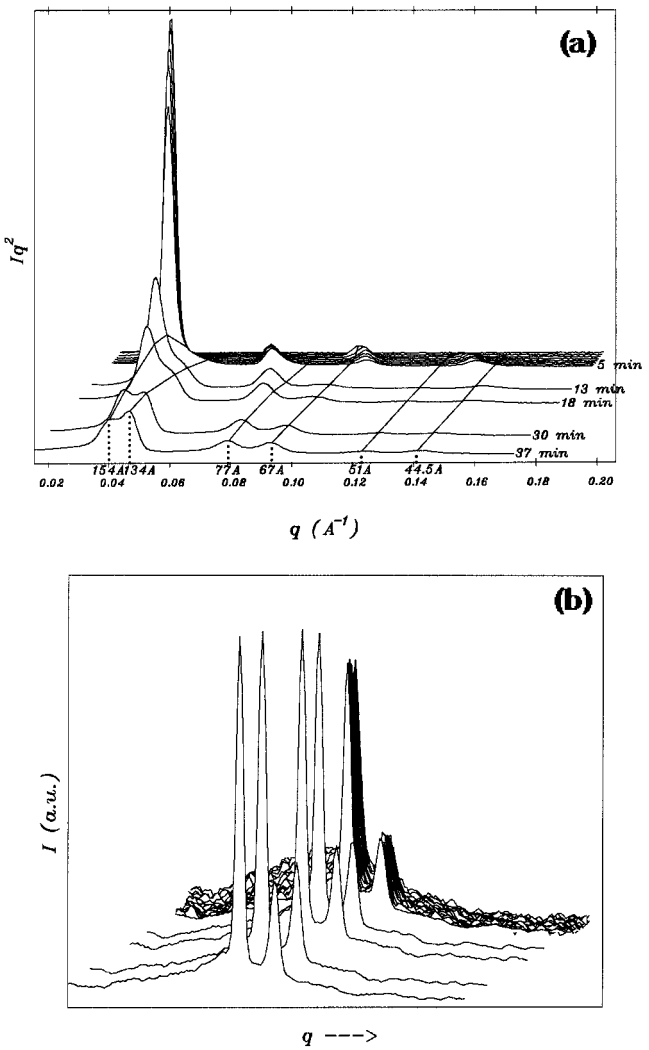

Figure 1. (a) Time evolution of SAXS during isothermal crystallization of *n*-alkane $C_{246}H_{494}$ at T_c = 111 °C from the melt. Time t is counted from the moment of reaching T_c. Abscissas are marked in q (in Å^{-1}) and $d = 2\pi/q$ (in Å). (b) Simultaneously recorded wide-angle diffractograms showing the 110 and 200 reflections of the orthorhombic lattice.

121 °C, respectively), *n*-alkane $C_{246}H_{494}$ crystallizes in the extended-chain form with chains tilted at 35° to the layer normal. Time-resolved SAXS experiments have shown that in this temperature region the alkane attains its final high degree of crystallinity in a single process:[10] neither the SAXS nor WAXD pattern changes noticeably after initial crystallization in an isothermal experiment. Below the extended-chain crystallization temperature range (i.e., below 121 °C in the case of $C_{246}H_{494}$) crystallization takes place in the NIF form;[6] here the SAXS patterns and their time evolution are fundamentally different. Figure 1a shows an isothermal series of SAXS diffractograms of $C_{246}H_{494}$ recorded in real time following a rapid temperature drop from 135 °C (melt) to T_c = 111 °C. The intense peak which forms first is the first-order NIF diffraction corresponding to a spacing of 194 Å. This value lies between that for crystals with tilted extended chains (calculated $L_0 = 315 \times \cos 35° = 257$ Å) and that for crystals with chains folded exactly in two (F2 crystals; theoretical spacing $L_0/2 = 129$ Å).

The appearance of the strong NIF diffraction peak is soon followed by a reduction in intensity and a simultaneous shift of the first and higher orders to larger wave vector q (i.e., to smaller spacings). At the same time, a second set of diffraction peaks appears, with the fundamental corresponding to a Bragg spacing L = 134 Å (i.e., 5 Å larger than the calculated theoretical $L_0/2$). This latter set is attributed to the F2 form.[6] As the wide-angle diffraction intensity from crystalline alkane increases only by a relatively small amount with time following the initial appearance of NIF (see Figure 1b), it is concluded that F2 forms through a gradual conversion of NIF.

The behavior of alkane $C_{198}H_{398}$,[11] and to some degree $C_{294}H_{590}$, is similar to that described above.

In the following two paragraphs, we give an outline of the method used to obtain electron density profiles (EDP). EDPs along the layer normals, $E(x)$, are even periodic functions and are thus related to diffraction amplitudes A_n by Fourier transformation as

$$E(x) = \sum_{n=0}^{\infty} A_n \cos(q_n x) = \sum_{n=0}^{\infty} A_n \cos\left(\frac{2\pi n x}{L}\right) \qquad (1)$$

Here $q_n = 4\pi \sin\theta/\lambda = 2\pi n/L$ is the wavevector of the n-th diffraction peak. The amplitudes are related to Lorentz-corrected diffraction intensities I_n as

$$I_n = |A_n|^2 \qquad (2)$$

Since the detector in our experiments captures only a limited number N of diffraction orders, the summation in (1) is only carried out to N and our EDP determined from experimental intensities, $E^E(x)$, suffers from truncation effects. To circumvent the problem, we devise model EDPs, $E^M(x)$, and then reconstruct them using the same N number of Fourier terms as the number of diffraction orders within the experimental range of the detector. The "truncated" EDPs thus obtained, $E^T(x)$, are then compared with experimental profiles $E^E(x)$ and a least-squares fit to the appropriate model is performed.

Three types of models were tried, a rectangular, a trapezoidal and a convoluted rectangular-Gaussian model.[9] The former two were found to be adequate for the cases studied presently. The rectangular EDP implies a simple two-phase model with sharp boundaries (model 1). Within the first period, it is defined as

$$E_1^M(x) = \begin{cases} E_0 & -L_c/2 < x < L_c/2 \\ 0 & \text{elsewhere} \end{cases} \qquad (3)$$

L_c is the thicknesses of the high-density phase, assumed crystalline; the thickness of the low-density "noncrystalline" layer is then $L_a = L - L_c$. The second, "trapezoidal" model (model 2) also contains two phases with an added transition layer of thickness L_s having a linear density gradient:

$$E_2^M(x) = \begin{cases} E_0 & (-L_c + L_s)/2 < x < (L_c - L_s)/2 \\ E_0(x + (L_c + L_s)/2)/L_s & (-L_c - L_s)/2 < x < (-L_c + L_s)/2 \\ E_0((L_c + L_s)/2 - x)/L_s & (L_c - L_s)/2 < x < (L_c + L_s)/2 \\ 0 & \text{elsewhere} \end{cases} \qquad (4)$$

The reported thicknesses L_c and L_a for model 2 are measured from center to center of the transition layer; hence, as for model 1, $L_c + L_a = L$. The fitting

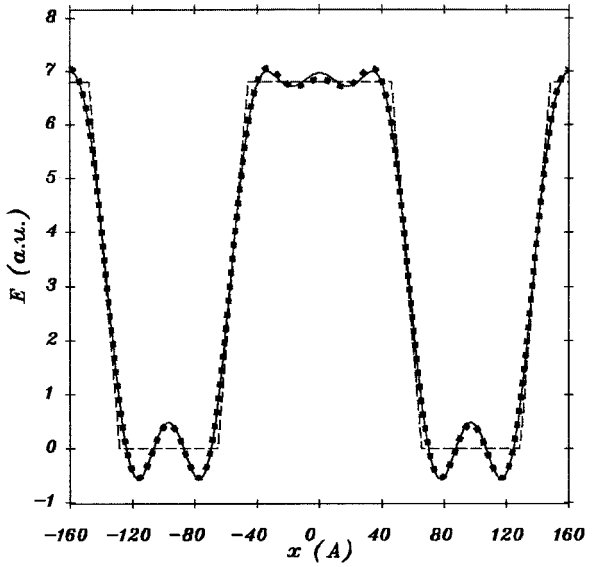

Figure 2. Experimental (E^E, solid curve), fitted (E^T, solid symbols), and best fit model electron density profiles (E_2^M, dashed) along lamellar normal for the initial NIF form ($t = 3$ min). For the origin at the center of the crystalline layer, the structure factor phases are $+ - - +$ for the first four diffraction orders ($- - + +$ if the origin is at the center of the noncrystalline layer). $A_5 \approx 0$.

parameters are L_c in the case of model 1 and L_c and L_s in the case of model 2.

The experimental, model, and truncated model electron density profiles, E^E, E^M, and E^T, are shown in Figure 2 for the NIF form soon after its formation (i.e., 3 min after the crystallization temperature had been reached). At this point, the initial sharp increase in crystalline WAXD peaks had ended (Figure 1b) and the first-order SAXS peak had reached the maximum (Figure 1a). Model 2 (trapezoidal) gives almost perfect coincidence between E^E and E^T for $L_c = 111$ Å and $L_a = 83$ Å with $L_s = 19$ Å ($L = L_c + L_a = 194$ Å). The ripples in E^E and E^T are caused entirely by truncation, in this particular case after the fifth Fourier term. The two phases with constant densities are interpreted as crystalline (L_c) and amorphous (L_a), the degree of crystallinity thus being only $L_c/L = 57\%$. It should be noted that the transition layer as obtained here contains not only genuine diffuseness of the crystalline-amorphous boundary, but also the imperfection in lamellar stacking.

The low initial degree of crystallinity, unexpected for a pure monodisperse linear alkane, is in fact consistent with the DSC measurements which show that only 61% of the heat of fusion of fully crystalline polyethylene is released in the crystallization exotherm in a cooling run of $C_{246}H_{494}$, giving NIF crystals.[19]

As already mentioned, with the progress of time at temperature T_c NIF diffraction intensity decreases, L decreases, and the NIF form is gradually converted into the discrete new once-folded integer form (F2). Electron density profiles were reconstructed for both phases at different stages. The reconstructed E^E profiles for the two coexisting forms at the end of the run ($t = 37$ min) are shown in Figure 3a. In both these cases, model 1 was used, as the improvement in using model 2 was insignificant. Figure 3b shows the corresponding best fit model EDPs (E^M), together with the E_2^M function for the as-formed NIF structure ($t = 3$ min). The fitting parameters are listed in Table 1.

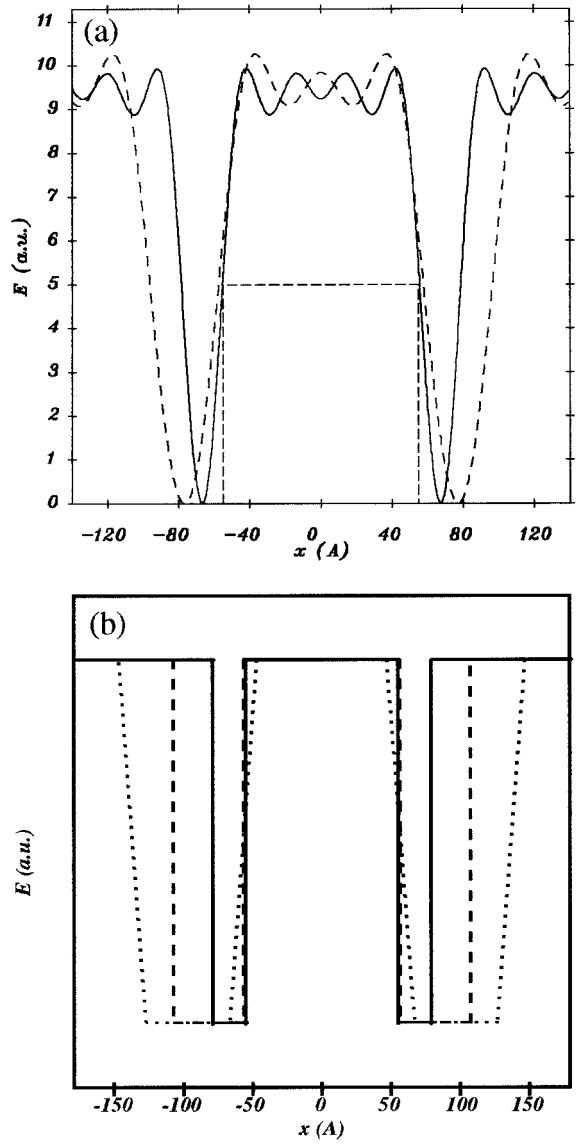

Figure 3. (a) Experimental electron density profiles (E^E) of NIF (dashed line) and F2 (full line) forms coexisting at the end of the isothermal crystallization experiment at 111 °C ($t = 37$ min, cf. Figure 1a). Structure factor phases are $+- ++$ for NIF and $+- + -$ for F2 ($- - -+$ and $- - -$, respectively, if the origin is at the center of the noncrystalline layer). (b) Best fit model profiles for NIF form at $t = 3$ min (E_2^M, dotted) and $t = 37$ min (E_1^M, dashed), and for the F2 form at $t = 37$ min (E_1^M, solid), all at 111 °C.

Table 1. Experimental Long Period (L) and Fitting Parameters (Crystalline, L_c, and Intercrystalline, L_a, Layer Thicknesses) for NIF and F2 Forms of n-$C_{246}H_{494}$ Isothermally Crystallized at 111 °C at Time t after the Onset of Crystallization

	L (Å)	model	L_c (Å)	L_a (Å)	L_s (Å)
NIF at $t = 3$ min at 111 °C	194	2	111	83	19
NIF at $t = 37$ min at 111 °C	154	1	103	41	
F2 at $t = 37$ min at 111 °C	134	1	109	25	
F2 at room temperature	130	1	110	18	

The intriguing features of the above EDPs is that in all cases the crystal layer thickness, L_c, is the same, within experimental limits. L_c remains constant in the NIF form while the overall periodicity decreases from 194 to 154 Å, and it maintains its value even as L drops to 134 Å upon the transition to the F2 form. The entire decrease in L is in fact due to a substantial decrease in

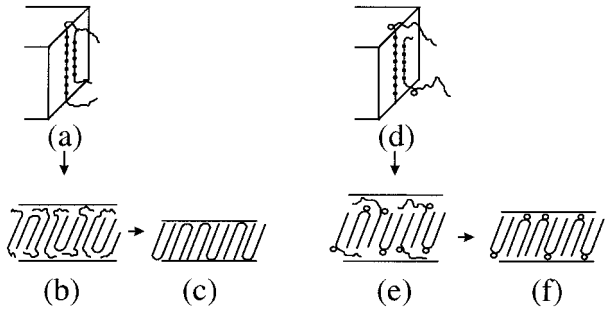

Figure 4. Schematic representation of molecular deposition on the crystal growth face (a,d), the NIF form (b,e), and the F2 form (c,f) for a linear alkane (a−c) and the branched alkane $C_{96}H_{193}CH(CH_3)C_{94}H_{189}$ (d−f).

the noncrystalline layer thickness. The L_a value of 25 Å for the F2 form (Table 1) is rather small and is comparable with the corresponding values for melt-crystallized extended-chain crystals of $C_{246}H_{494}$ and $C_{194}H_{388}$ at comparable temperatures.[9] On cooling to room temperature L_a for the F2 form reduces reversibly to only 18 Å. $L_a/2$ can be taken as the thickness of one-fold surface layer; its value of only 9 Å indicates a comparatively high regularity of folds in the integer once-folded form. A fold layer of similar thickness is observed in solution-grown F2 crystals[12]—see also ref 11.

On the basis of the above results, our interpretation of the NIF form and of the way chain-folded crystallization takes place from the melt is as follows—see Figure 4a−c. To account for the large fraction of uncrystallized interlamellar material in the NIF form, we propose that only some of the molecules are folded and have both their halves within the crystalline layer. Other molecules are only half-crystallized, traversing the crystal layer only once. They are not folded and their noncrystalline halves (cilia) remain outside the crystals, forming the amorphous layers. The structure is drawn schematically in Figure 4b. As in melt-grown crystals of integer forms, crystalline chain stems in NIF are tilted within the crystal layer; hence, L_c is the same as in the (tilted) F2 form and corresponds to half that in the extended-chain crystals.[9] Accordingly, those chains in the NIF form that are folded are in fact integer-folded (folded exactly in two). Such a NIF structure enables a separation of crystalline and amorphous phases along a sharp boundary.

We can make an estimate of the fraction of folded molecules in the NIF form from the knowledge of the volume ratio of amorphous and crystalline layers and applying the values for crystalline and amorphous densities for polyethylene (i.e., 1.00 and 0.85 g cm^{-3}, respectively. We are not likely to make a significant error in assuming that all molecules are folded in the F2 form. Thus, we take the measured L spacing of $F2$, L_{F2}, as the baseline and the difference $L_{NIF} - L_{F2}$ we attribute to the cilia layer. If χ is the mass fraction of folded chains, then

$$\frac{1-\chi}{1+\chi} = \frac{0.85(L_{NIF} - L_{F2})}{L_{F2}}$$

With $L_{NIF} = 194$ Å for as-formed lamellae and $L_{F2} = 134$ Å, $\chi = 0.44$. Thus, just under half the molecules in the initial crystals are folded and traverse the crystal layer twice. This fraction increases to three-fourths (0.77) in the NIF form which remains at the end of the isothermal run at 111 °C; however, the majority of the material is by then contained in the fully folded F2 form (note that the scattering power of F2 is intrinsically lower than that of NIF).

In their work on isothermal crystallization of PEO fractions using Raman spectroscopy Kim and Krimm[13] find an initial LAM band corresponding to a straight-chain segment length intermediate between the full- and the half-chain length. After prolonged annealing this NIF band gives way to extended-chain and F2 bands. This result is in apparent disagreement with our model according to which a NIF structure would give a LAM frequency corresponding to half the chain length. Indeed, in all our previous work on alkanes we only ever observed LAM bands corresponding to integer folding. Thus, a melt-quenched and a solution-crystallized sample of $C_{246}H_{494}$ both gave the LAM frequency exactly twice that of the extended-chain sample (i.e., corresponding to half the chain length), even though the former sample had a significant proportion of trapped NIF form while the latter was purely F2.[4,11] At present we can only speculate about the possible reasons for the observed difference between the alkane and PEO results.

Figure 4a illustrates our proposed mechanism of formation of a NIF lamella. During crystal growth a chain attaches half its length to a growing crystal randomly along its length. However, if the chain is to fold back and have its other half crystallized, its starting position must be at a basal crystal surface. Since irregular deposition is significantly more probable, provided the resulting conformation is stable at the given crystallization temperature, NIF rather than IF crystals develop. There is a possibility of subsequent rearrangements of a partially attached molecule, leading to a fully crystallized once-folded conformation. However, it is likely that these are hampered by other molecules partly or fully occupying the neighboring sites—see Figure 4a. Nevertheless, as is well-known, in order for a lamella to grow to infinite lateral dimensions at least half the crystallized stems must either terminate or fold back on reaching the basal surface for steric reasons. This requirement alone must favor once-folded chains above the probability based on random attachment. Indeed as derived above, even in the as-crystallized NIF form chain-folded molecules make almost half of the total number. In fact, maintaining the minimum required proportion of regularly folded chains may be controlling the rate of lamellar growth.

The fact that competition for neighboring sites from other molecules is reduced in crystallization from a dilute solution is, according to the above mechanism, consistent with the fact that no evidence of NIF has been observed in solution-grown crystals of long alkanes.

Further support for the above mechanism comes from crystallization experiments on alkane $C_{96}H_{193}CH(CH_3)$-$C_{94}H_{189}$ which contains one methyl branch in the center of the otherwise linear chain (for details on synthesis see ref 8). This alkane persistently gives F2 crystals. Neither extended nor twice-folded chain (F3) crystals could be grown either from melt or solution, indicating a strong tendency for methyl branches to be segregated to the lamellar surface.[14] However, time-resolved SAXS experiments do reveal a brief appearance of the NIF form. Figure 5 shows SAXS traces recorded at 12 s intervals during isothermal crystallization of $C_{96}H_{193}$-

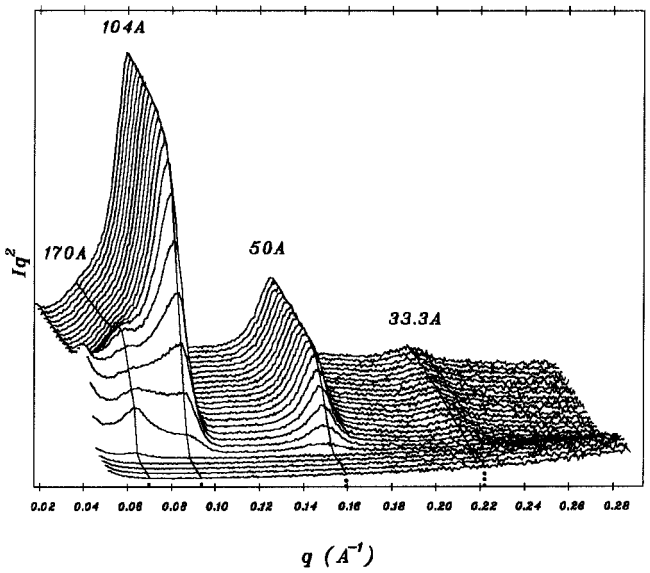

Figure 5. Time evolution of SAXS during isothermal crystallization of branched alkane $C_{96}H_{193}CH(CH_3)C_{94}H_{189}$ at $T_c = 110$ °C from the melt. 12-s time frames starting from front to rear. T_c was reached in frame 4.

$CH(CH_3)C_{94}H_{189}$ at 110 °C. The appearance of NIF diffraction peak at $L = 170$ Å is succeeded almost immediately by the emergence of the 104-Å peak of the F2 form (theoretical $L = [191 \times 1.27 + 2]\cos 35° = 100$ Å). The F2 form (second-diffraction order, 50 Å; third order, 34 Å) soon takes over and NIF disappears within about a minute of the onset of crystallization. Diffraction intensity of the NIF form never builds up to more than a small fraction of that in linear alkanes, taking F2 intensity as reference. This is consistent with a high rate of NIF → F2 transition in the sequence of consecutive transformations melt → NIF → F2.

We attribute the high rate of the NIF → F2 transition in $C_{96}H_{193}CH(CH_3)C_{94}H_{189}$ to the fact that here the only successful deposition mode of the first stem (first half) of the molecule is one which places the branch at one lamellar basal surface and the chain end at the opposite surface—see Figure 4d. This leaves the molecule with only one uncrystallized cilium, the length of which is precisely half that of a full chain. Such a cilium is ideally suited to complete a second traverse of the crystal. Thus, although many such cilia remain uncrystallized during primary formation of the lamellae, giving rise to the NIF form (Figure 4e), when they subsequently enter the crystal, the formation of the stable F2 conformation is relatively straightforward (Figure 4f). In contrast, in a NIF lamella of a linear alkane a half-crystallized molecule generally has two cilia, neither of them long enough to complete a second traverse without rearrangements involving the whole molecule, including the already crystallized part. In the sequence melt → NIF → F2, the melt → NIF step is fast but the NIF → F2 step is slow in linear alkanes. The reverse is true for the branched alkane.

The above results give further insight into the mechanism of crystallization of polymer chains and on postcrystallization events. Particularly intriguing are the high self-diffusion rates implicit in the observed NIF → F2 transformation process. Further work is in progress.

Acknowledgment. The authors thank the Engineering and Physical Research Council for financial help and Drs. B. U. Komanschek and E. Towns-Andrews for their help with setting up the SAXS experiments.

References and Notes

(1) For a review see: Buckley, C. P.; Kovacs, A. J. In *Structure of Crystalline Polymers*; Hall, I. H., Ed.; Elsevier Applied Science Publishers: London, 1984; p 261.
(2) Bidd, I.; Whiting, M. C. *J. Chem. Soc., Chem. Commun.* **1985**, 543.
(3) Lee, K.-S.; Wegner, G. *Makromol. Chem., Rapid Commun.* **1985**, *6*, 203.
(4) Ungar, G.; Stejny, J.; Keller, A.; Bidd, I.; Whiting, M. C. *Science* **1985**, *229*, 386.
(5) Ungar, G. S. J.; Organ, S. J.; Keller, A. *J. Polym. Sci., Polym. Phys. Ed.* **1988**, *26*, 259.
(6) Ungar, G.; Keller, A. *Polymer* **1986**, *27*, 1835.
(7) Cheng, S. Z. D.; Zhang, A.; Chen, J.; Heberer, D. P. *J. Polym. Sci., Part B: Polym. Phys.* **1991**, *29*, 287; Cheng, S. Z. D.; Chen, J. *J. Polym. Sci., Part B: Polym. Phys.* **1991**, *29*, 311.
(8) Brooke, G. M.; Burnett, S.; Mohammed, S.; Proctor D.; Whiting, M. C. *J. Chem. Soc., Perkin Trans. 1* **1996**, 1635.
(9) Zeng, X.; Ungar, G. *Polymer* **1998**, in press.
(10) Ungar G.; Keller A. *Polymer* **1987**, *28*, 1899.
(11) Ungar, G. In *Integration of Fundamental Polymer Science and Technology*: Lemstra, P. J., Kleintjens, I. A., Eds.; Elsevier: London, 1988; Vol. 2, p 346.
(12) Zeng, X.; Ungar, G.; Boda, E., to be published.
(13) Kim, I.; Krimm, S. *Macromolecules* **1996**, *29*, 7186.
(14) By rapid melt quenching it is however possible to temporarily freeze some NIF form at room temperature.

MA971539T